LHCb 2000-036
CALO
21 June 2000

The Hadron Calorimeter Prototype Beam-test Results

C.Coca, T.Preda, A.Rosca (IFIN-HH, Bucharest, Romania),
I.Ajinenko, A.Dorokhov, R.Dzhelyadin, A.Konoplyannikov, V.Matveev, V.Novikov,
O.Yuschtchenko (IHEP, Protvino, Russia),
Yu.Ranyuk (KhIPT, Kharkiv, Ukraine)

ABSTRACT

Here We present here the beam-test results obtained with the HCAL Prototype exposed on the X7 beam line of the CERN SPS accelerator. The iron plate – scintillator tile sampling calorimeter has been tested in the beam momenta range $10 \div 80$ GeV/c.

The measured energy, angular and coordinate dependences of the HCAL responce and resolution were found to be corresponding to the LHCb design requirements. The angular and X-Y coordinate uniformity have been checked and compared with stand-alone Monte-Carlo simulation program predictions.

The radioactive source calibration procedure has been developed. The LED pulse system allows to monitor the short-term stability of the detector.

New 40 MHz front-end electronics have been tested and compared with ordinary charge integrating ADC's. The results of the first combined calorimeter tests are also presented. The signal shapes have been studied for HCAL, instrumented with different fiber types and were found to satisfy the LHCb performance requirements.

1 Introduction

The purpose of the hadron calorimeter (HCAL) in the LHCb experiment [1, 2] is to provide data for the trigger and to assist in background suppression on reconstruction of B decays. The overall dimension of the active area of the detector is foreseen to be $8.4 \times 6.8\text{m}^2$ [3].

The technology chosen for the HCAL design is a scintillator/iron sampling structure with scintillating tiles arranged in parallel to the beam axis. This structure has been already tested in the ATLAS TileCal [4] design. It incorporates several advantages:

- the 'natural' iron spacer length between tiles in the longitudinal direction of the order of hadronic interaction length λ_I,
- in the transverse direction iron thickness between tiles is of the order of one radiation length, X_0, suitable for electromagnetic cascade development,
- the fibers run along the calorimeter depth and have a large contact surface with the tiles, providing efficient light collection,
- the calibration system is easily inserted in the calorimeter volume without causing insensitive zones.

During the HCAL Prototype [5] construction in 1997-99 several variants of the detector shown in Fig. 1 have been realised.

They differ by the cell size (8 cm and 16 cm), by their depth ($7.3\lambda_I$ and $5.6\lambda_I$) and by different light collection schematics (double and single sampling in depth) and have been equiped with two types of fibers: Pol.Hi.Tech.(S250) and BICRON BCF-92.

The different prototypes allow to perform a study of the optimal final design.

This note presents the beam-test results with HCAL essential for it's performance check and for designing the full scale detector.

2 The energy dependence of the response

In general sampling calorimeters show a linear dependence of energy response. But some precautions have to be taken in the detector design to reach this goal. In practice the result is obtained by compromising between the required performance and the simplicity in construction.

The choise of iron plates as a passive radiator is an illustration of the above. It is known that iron calorimeters are non-compensating. This feature is caused by a rising fraction of π^0's with an energy: $\pi^0/\text{all} \sim 0.23 \ln(E)$, ($E$ in GeV), that results in an increase of detected energy E with respect to the incident particle energy E_b:

$$E/E_b \approx 1 + \gamma \ln(E_b/E_c)$$

,

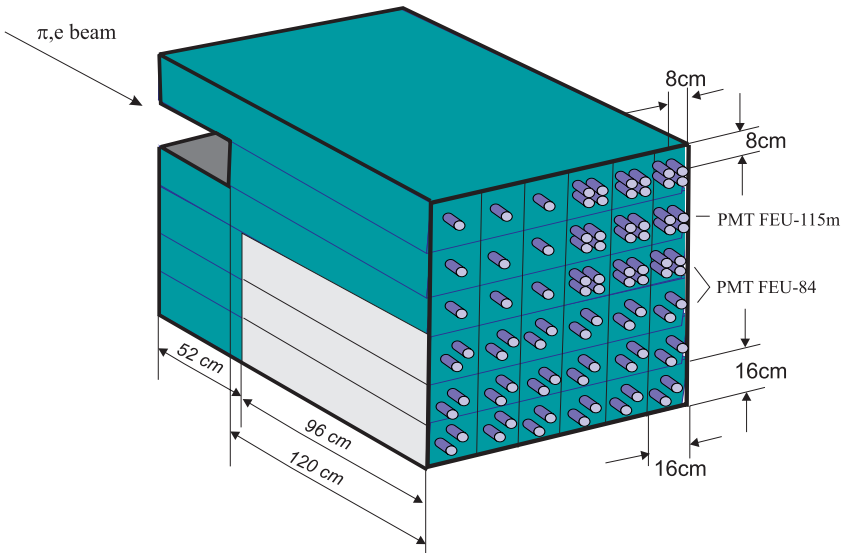

Figure 1: The HCAL Prototype general view. Three bottom modules aredouble-segmented in depth. Three top modules have no segmentation in depth, instead were divided in part on to four smaller cells. Different PMT's shown were used for light collection.

where E_c is the calorimeter responce calibration energy point.

The other source of non-linear behaviour could be the shower leakage behind the detector. This causes two opposite effects: it decreases the detected energy due to leakage, but on the other hand, it can generate Cerenkov light in the fiber bundle just in front of the PMT. To investigate this phemomena we use the advantige of two thickness of the prototype, 7.3 and $5.6\lambda_I$ for the comparison of the measured quantities.

Hadrons from B-meson decays accepted in the LHCb detector have mostly moderate momenta below 100 GeV and the calorimeter resolution is dominated by the sampling term. One can expect that in this energy range the main source of non-linearity is the attenuation in the fiber running along the calorimeter depth, gathering light of several tiles. High energy showers in average deposit energy closer to the PMT then low energy showers, thus resulting in a larger signal responce.

Here an attempt is made to exclude the systematic distortion in energy response caused by fiber attenuation. The average energy dependent shower maximum located at depth Z_{max} is given by $Z_{max}/\lambda_I = 0.2\ \ln(E) + 0.7$.

If the total calorimeter length is L_0 then a distance L between the average shower maximum and the PMT is given by:

$$L = L_0 - Z_{max} = \alpha - \beta \ln(E/E_c)$$

and light generated at this distance is attenuated (in the fiber with an attenuation length

λ_{att}) by an exponential factor:

$$A(L) = A_0 \exp(-L/\lambda_{att})$$

As mentioned above the increase in π^0's with energy results in a smooth logarithmic behaviour

$$A_0 \approx (1 + \gamma \ln(E_b/E_c))$$

Then the energy E measured by the calorimeter is related to the incident particle energy E_b:

$$E = k\, E_b\, [1 + \gamma\, \ln(E_b/E_c)] \left(\frac{E_b}{E_c}\right)^{\beta/\lambda_{att}}$$

where k - is a calibration coefficient measured at energy E_c and γ - is related to the e/h-ratio. Looking at this formula it is evident that the correction factor caused by attenuation is diminished if λ_{att} becomes large enough, e.g. infinitely large, if we take special action to compensate the increase in light yield with depth. This procedure has been applied to one of the Prototype modules. We reduced the length of the optical contact between fiber and tile at the corresponding depth (originally it was 157 mm) by several percent (pieces of black paper of $6, 12, 18, 24$ and 30 mm have been inserted). In principle, using this procedure we can obtain any effective λ_{att} we want, even negative.

Fig. 2 shows the deviation from the linearity of the calorimeter response for a module without compensation for hadron beam energies of $10 \div 80$ GeV. Open points show data before correction, and black points after the correction has been applied as given by the formula above.

There are several consequences of the given analysis:

- the correction to be applied is rather small, within $sim1$ GeV for whole energy range of interest;

- corrections if needed, could be easily implemented in energy evaluating look-up tables both at the trigger level and in further data analysis;

- understanding of the calorimeter responce nature can help in correction of the attenuation effect caused by the radiation damage of fibers during LHC operation. Those effects could be easily monitored using radioactive source calibration.

3 Angular dependence of response

The angular dependence of the HCAL Prototype response has been studied at different energies of the incident beam. For that measurement the Prototype has been rotated around the vertical axis located roughly at the shower maximum. Modules 4 and 5 (counting from bottom on the Fig. 1) have been used for this study.

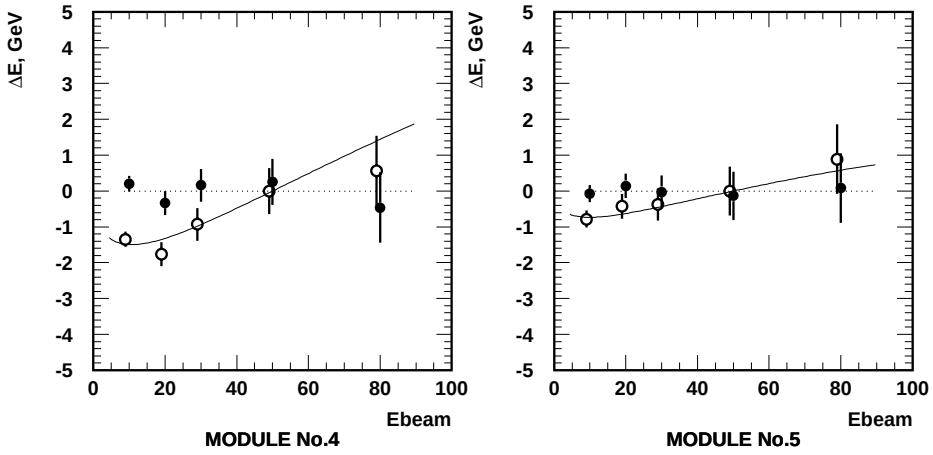

Figure 2: The difference between the mean measured energy and the beam energy (calibration at 50 GeV). Open circles — raw data before correction. The curve is a fit to points by the formula discussed in the text, i.e. correction function. The black circles are the same points after correction. Left figure without compensation, right figure with compensation for light attenuation. The correction become smaller but remain non-zero that is accounted for by a smooth logarithmic rise of the π^0 fraction in the shower. The data was taken at 9^0 of incident beam.

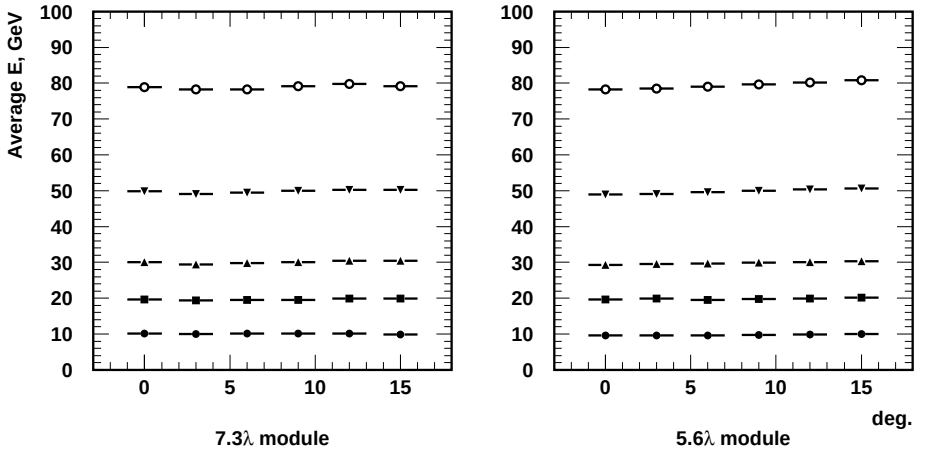

Figure 3: The angular dependence of the response at different energies. The X-axis is an angle between the beam line and the perpendicular to the HCAL front face. The smooth $\sim 3\,\%$ decrease in response at highest energies for the short module is accounted for leakage effect (see text).

Fig. 3 shows two sets of data collected with prototype thickness of $7.3\lambda_I$ and $5.6\lambda_I$ respectively. A prominent uniformity is seen. At higher beam energies, the short module shows $\sim 3\,\%$ leakage at small angles that is specific to stand-alone HCAL beam-test. Taking into account that in the LHCb detector the ECAL adds another $1.2\lambda_I$ in front of HCAL, the total thickness will amount to $6.8\lambda_I$. The precise measurement with high statistics is foreseen for the combined beam-tests in the future.

4 The calorimeter resolution

The energy dependence of the resolution for sampling hadron calorimeter is described by two parameters: the stochastic and the constant term. The first reflects the statistical fluctuation in the energy deposition by hadronic showers in the scintillating tiles. The second one is defined by intrinsic features of the calorimeter, like inter-calibration, nonuniformity in the light collection for different fibers in the cell, non-linear response due to shower fluctuations in depth, energy leakage, cracks and so on.

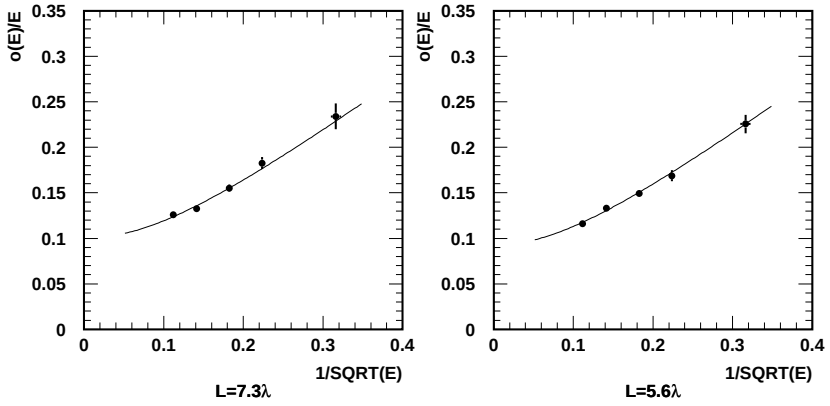

Figure 4: The resolution as a function of beam energy for two prototype depth. Data taken at 9^0. The curve is the fit.

The measured resolution for two prototype modules with different length is shown in Fig. 4. The data have been fitted by the quadratic sum of stochastic and constant term:.

$$\sigma(E)/E = (0.65 \pm 0.06)/\sqrt{E} \oplus (0.10 \pm 0.02), \quad \text{for} \quad L_0 = 7.3\lambda$$
$$\sigma(E)/E = (0.67 \pm 0.05)/\sqrt{E} \oplus (0.09 \pm 0.02), \quad \text{for} \quad L_0 = 5.6\lambda$$

The angular dependence of the resolution is shown in Fig. 5. A good uniformity is obtained within the experimental errors. The results have been extracted by a gaussian fit to the energy spectra within $\pm 25\,\%$ of the peak value. This procedure introduces

some systematic uncertainty estimated to be 5 % and has been quadratically added to the statistical error.

The small rise at high energies is due to the Cerenkov light generated in the fiber bundles and light mixers by the shower leakage at the rear side of the detector.

In our final design a care could be taken to minimize this effect, e.g. light mixers can serve as a short wave-length filters. This will reduce both Cerenkov light and the decrease in the fiber transparency as mentioned in [6]. Again, in the final set-up an ECAL of $1.2\lambda_I$ will certainly reduce the leakage effects.

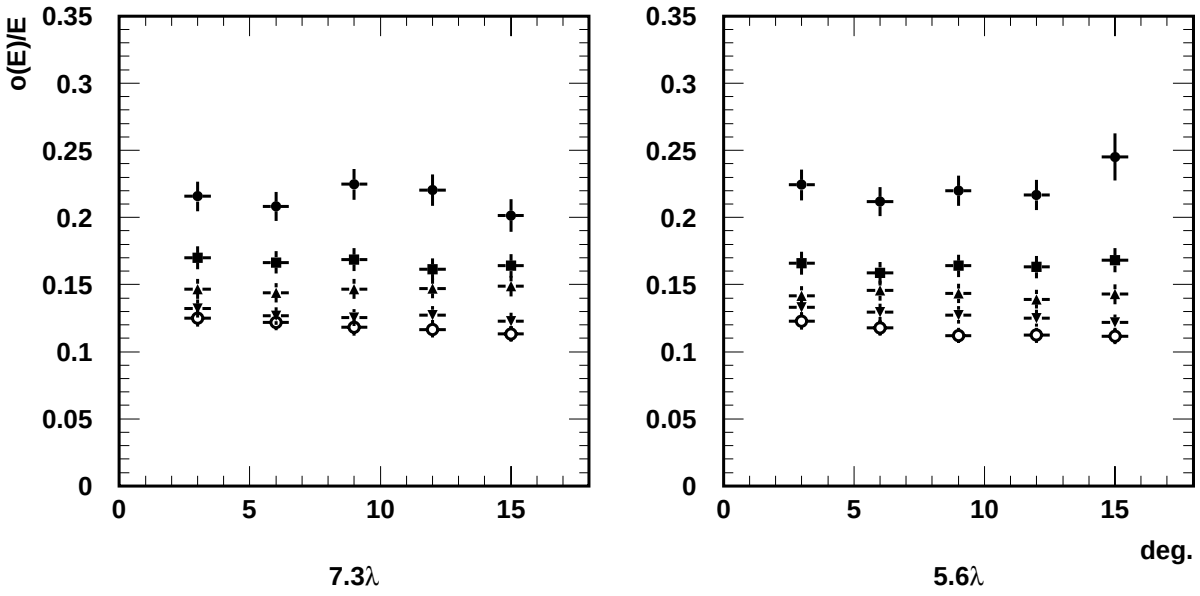

Figure 5: The angular dependence of HCAL resolution for two prototype thickness. Each set of points correspond to the beam energy of: 10, 20, 30, 50 and 80 GeV (from top to the bottom).

5 The uniformity of response

The study has been done with a beam scan along the X- and Y-coordinates. Here we take advantage that the Prototype has almost one square meter of front surface. Fig. 6 shows the uniformity of response for the scan in X (horizontal) direction.

The uniformity of response is within ± 5 %. On the next Fig. 7 the Y-scan across small cells is shown. Those tiles have been cut into two equal pieces and each half read out by one independent fiber. One could expect some non-uniformity due to light attenuation in the scintillating tile at the center of each module. Another source is the non-instrumented (for fiber path) crack zone of $\sim$ 3 mm between the modules. Such cracks could also deteriorate the resolution, but no evidence of this is seen in Fig.7.

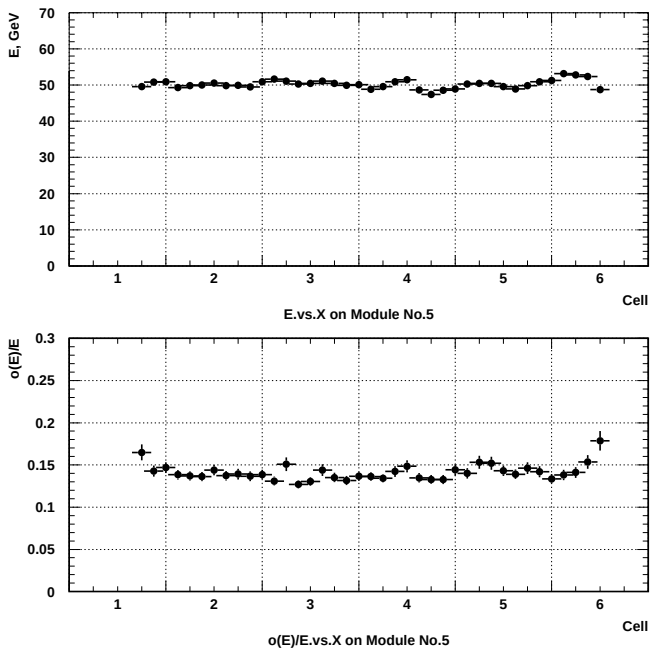

Figure 6: The response of the HCAL prototype to a X-scan. Top - the signal response, bottom - the resolution dependance. Thickness $5.6\lambda_I$, beam angle 3^0.

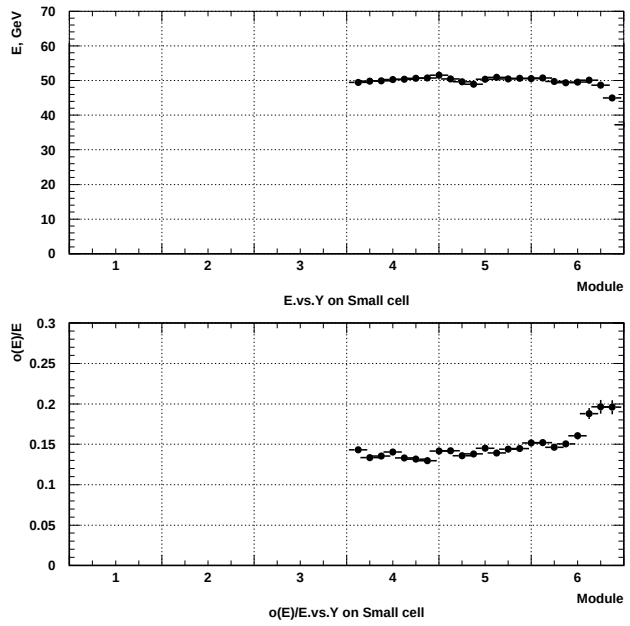

Figure 7: The response of the HCAL prototype to a Y-scan (X-axis is a module number). Only upper half with small cells have been scanned however whole HCAL have been operational and were used for energy reconstruction. The beam angle is 3^0 of the energy 50 GeV.

In the module 6 (right side on Fig. 7) there is a degradation caused by the shower leakage outside the detector. This border effect is contained within the small region of 10 cm near the external calorimeter side.

The average hadronic shower profile both X- and Y-directions have been deduced from the scan data. The formula used is:

$$P(X) = \frac{\Delta}{\Delta X}\left(\frac{\sum_{i\in HALF} E_i}{\sum_{i\in WHOLE} E_i}\right)$$

where X – is the beam position with respect to an imaginary vertical plane dividing HCAL onto two parts, $\Delta X = 2\,\mathrm{cm}$ is the scan step. The formula represents the fraction of energy deposited in the half of HCAL depending on the beam position.

The same procedure has been applied to sum over two halfs in Y. The hirizontal plane have been chosen between the 4-th and 5-th module. Care have been taken to reject muons and splashes caused by interactions upstream of the detector.

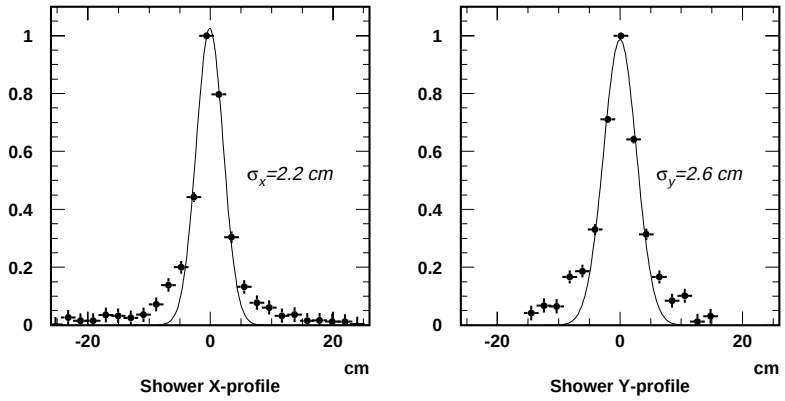

Figure 8: The average hadronic shower profile in X- and Y-directions. To select hadron showers a cut of $0.5 < E/E_{mean} < 1.5$ has been applied.

The beam size was $\sigma_{x,y} \approx 1.2\,\mathrm{cm}$, and the scan was done with 2 cm steps.

The prominent central core is seen in the shower profile, however it can not be described by a single gaussian. The tail caused by fluctuations results in 95 % of the deposited energy are contained within $(27 \pm 3)\,\mathrm{cm}$ in both horizontal and vertical directions.

6 The calibration procedure

In the first years of the beam tests before developing a radioactive source calibration as discussed below, we use a 50 GeV pion beam to calibrate whole prototype. The procedure took several hours to scan over all cells in the beam. This procedure was iterative, with

HV correction and re-calibration. The inter-calibration of all channel has been reached in 2 or 3 attempts with tolerance better than 15 %.

The second step was the linearity calibration of the LeCroy 2249W 11-bit ADC's. The precision ADC-Tester (LeCroy 1976) was used to inject a variable calibration charge in each channel. Minor non-linearities in the ADC electronic modules has been corrected by the parabolic approximation during data processing:

$$E = k[A + 4\alpha X(1 - X)], \qquad X = A/A_c$$

here A is the digitized signal to be corrected, α and A_c are parameters specific for each ADC input. The parameter α as large as $1 \div 4$ have been applied for correction. This value was non-negligable taking into account the typical PMT gain setting of $1/k \sim 4 \div 6$ ADC-channels/GeV.

We then developed a calibration using a radioactive source. A miniature Cs^{137} radioactive source was used, encapsulated in 2 mm diameter 4 mm long stainless steel tube welded at both ends. The source was driven by the hydraulic system, filled with a distilled water. The system includes a set of pipes fed through all scintillating tiles in the calorimeter, a garage to safe the source and a computer controlled pamp and valves that allows to reverse the water flow direction.

The source activity of 5 mCi was enough to induce in the PMT a current up to 90 nA being integrated by a slow control electronics circuit. The integration time does not exceed 2 ms and the readout of all PMT channels is repeated each 5 ms.

The average source velocity is within range of $20 \div 40$ cm/s. The calibration results are independent of the source speed.

The typical shape of the recorded PMT current is shown on Fig.9

The calibration procedure includes a fit of the shown PMT response by the empirical function:

$$I(x) = \sum_{i=1}^{N} p_i \left(\frac{0.9}{1 + 2.0(x - i\Delta x)^2} + \frac{0.1}{1 + 0.1(x - i\Delta x)^2} \right)$$

with p_i – the fiber contribution weight, $\Delta x = 2\,\mathrm{cm}$ – the distance between tiles, N – number of fibers in the particular cell. The two parts in the chosen function reflect the tile response to the gamma flux at the short and long distances. The black points on Fig. 9 are the parameters p_i - the result of the fit. Two additional free parameters have been used in the fit to allow an overall X-shift and source speed (X-scale factor) adjustment.

The stainless steel pipe of 8 mm outer diameter guiding the Cs^{137} source has been fed through each calorimeter cell several times at different depth. This allows to measure the signal response at different distances to the PMT and to monitor the fiber attenuation length. Fig. 10 shows the measured relative yield of the PMT current as a distance to the PMT in three cases: left – without compensation of the light yield due to attenuation in the fibers, central — with compensation and right – with irradiated fibers and tiles up to dose of $(0.6 \div 0.8)$ Mrad.

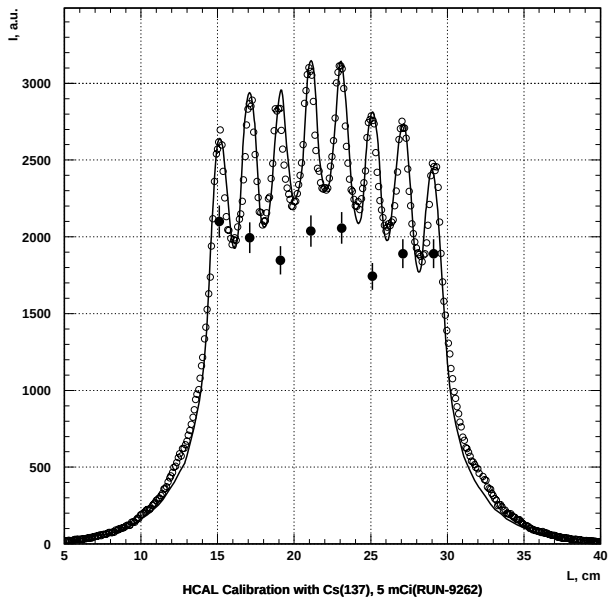

Figure 9: The radioactive source induced PMT current.The X-axis represents the moving source position. The peaks correspond to the tile locations. Open circles are the current measurement data (repeated each 5 ms). The line represents the fitting curve obtained as a sum of the single tile response, displaced by a 2 cm period. The black points are the fit parameters (see text), reflecting the contribution of each tile to cell signal.

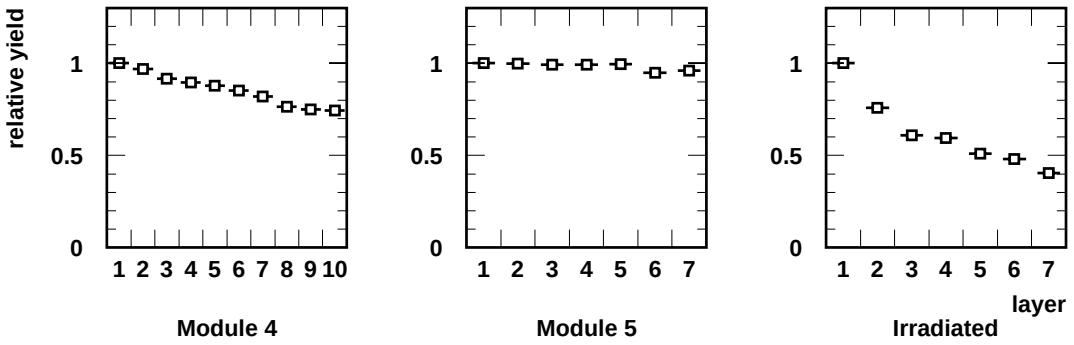

Figure 10: The radioactive source calibration data. The relative tile yield dependence on it's distance (layer number) to the PMT for three different cells. Odd layers and even layers are averaged over their own set of fibers due to the HCAL internal structure. Left figure – Pol.Hi.Tech (S250) fiber without compensation. The estimated attenuation length exceeds 4 m. Central – BCF-92 fibers compensated. Tiles in each consecutive layer are attenuated with 6 % increment. Right – Pol.Hi.Tech (S250) fibers and tiles pre-irradiated up to 0.8 Mrad with hadron showers.

The last figure shows what is expected after 10 to 15 years of HCAL operation in the central cells. This have been done with tiles and fibers pre-irradiated at the Serpukhov proton synchrotron upto 0.8 Mrad dose and incerted after in the HCAL Prototype. The individual tile irradiation level have been measured and they were arranged to follow the dose change with depth in the LHCb HCAL environment.

The relative yield measurement shown in Fig. 10 is independent of the absolute gain (or high voltage on PMT) setting and allows to monitor the fiber-tile degradation process in time.

We compared the two independent calibrations done with beam particles and the radioactive source, and a tolerance within 10 % has been achieved easily in the central calorimeter cells. The agreement between the two calibration procedures is better for those cells that have been compensated for attenuation in fibers. Further development of this procedure is in progress.

The calibration system willd be used during the assembly of the HCAL modules. Damaged fibers can be recognized at an early stage of assembly and replaced. The corresponding tools are currently under design, e.g. a stand-alone prototype of slow control sub-system for reliable measurements.

The radioactive source calibration is expected to be operated with rather long time intervals. Between those measurement the stability of the HCAL will be checked by a pulsing LED system.

The prototype of this subsystem has been implemented and tested. The major task is the PMT gain stability monitoring. The second task is to monitor the HCAL sensitivity. The pulse height of the LED is controlled by the computer that allows to measure the HCAL response in terms of photo-electrons per GeV of the deposited energy. The HCAL Prototype sensitivity was found to be around $30 \div 50$ photo-electrons/GeV. This value is well above the level where photo-statistics would dominate the HCAL resolution.

Another task for the LED subsystem is the synchronization between different PMT channels. The detailes of it is currently under development. Bright blue LED's with required timing properties become available recently. The special short-pulse LED-driver have been developed for that purpose and tested.

The third task for the LED subsystem is the PMT-electronics chain linearity check. The goal is achieved with two independent LED's joint together in each module. This procedure was tested during the PMT's linearity study [7] and is currently under design for the final HCAL implementation.

7 The Monte-Carlo simulation

The stand-alone Monte-Carlo simulations has been performed with the detailed description of the calorimeter structure. Several set-ups have been simulated: the HCAL alone, the homogeneous ECAL 40 cm upstream of HCAL and full calorimeter system with SPD/Pb-Converter/PS preshower detector (each layer of 1 cm thick) in front of ECAL.

A square 5×5 cell HCAL model has lateral cell dimension of $16 \times 16\,\mathrm{cm}^2$ and both

7.3 and 5.3 λ_I thick. Each cell has been divided in 5 volumes in depth (two tile layers per volume) and the energy deposited in the tiles has been recorded in a 3-dimensional array.

The beam incident point was smeared randomly over 6 zones ($8 \times 8\,\mathrm{cm}^2$) that overlap within the central cell. The beam incident angle was generated at $\theta = 0.020, 0.040, 0.080$ and 0.160 rad and $\phi = 0^o, 45^o$ and 90^o with respect to the horizontal plane.

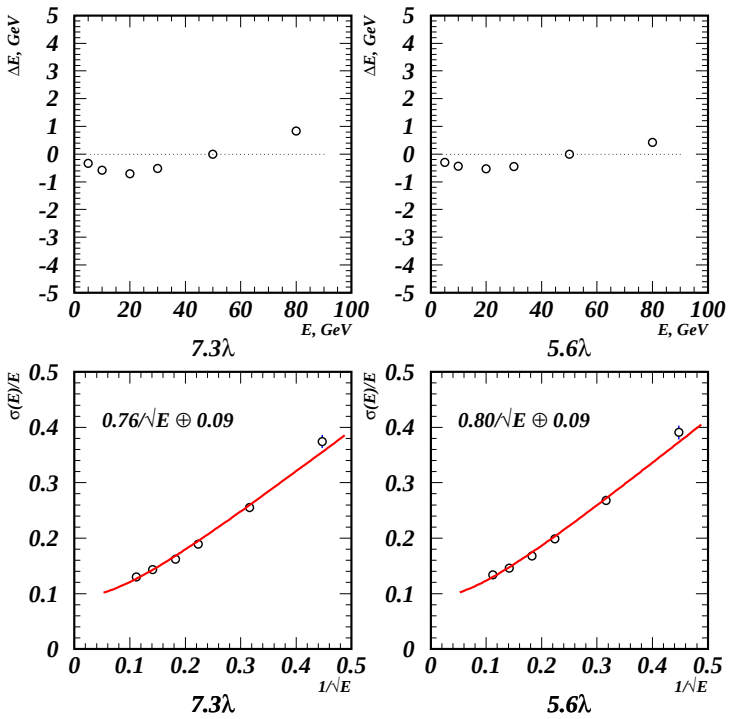

Figure 11: The Monte-Carlo simulated deviation from linear response and relative resolution as a function of the incident particle energy. The data are very like to those in Fig. 2 and Fig. 4, measured with the existing Prototype. Left – 7.3λ, light attenuation in fiber simulated. Right – 5.6λ, the equal light yield through depth. Minor non-linearity remain due to e/h non-compensation in iron.

For each angle setting only 6000 events were generated (1K event per zone) due to large consumption of computing time, especially at higher energies. The primary pions have $E_b = 5, 10, 20, 30, 50$ and 80 GeV. A few points were generated at $E_b = 100$ and 200 GeV both with electrons and pions as a primary particle.

We use standard GEANT 3.21 version with GEISHA program for showers with 1 MeV cut on electrons/gammas and 10 MeV for hadrons. The total volume of generated ntuples exceeds 1 Gbyte of the disk space.

The linearity of the calorimeter response as well as the energy dependence of the resolution have been checked. Those results are shown in Fig. 11 for both calorimeter

thickness. A small non-linear behavior is seen like in the real data that has been shown in Fig. 2. It happens due to the inherent feature of the iron sampling calorimeter and is correctly described by the MC simulation. The energy behaviour of the resolution also looks quite similar to the real data shown in Fig. 4, except for sampling term that is $10 \div 15\,\%$ larger than measured in the beam test. This effect of GEISHA has been already metioned in [8]. The constant term for both generated and real data coincides within $10\,\%$.

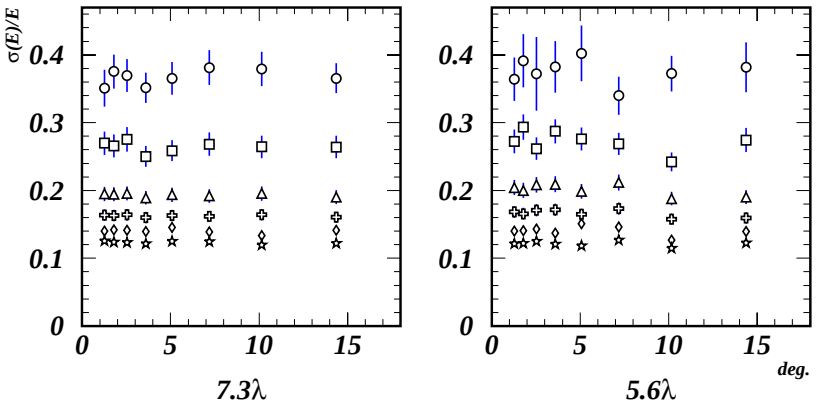

Figure 12: The Monte-Carlo simulated angular dependence of the resolution. The used energy range: $E = 5, 10, 20, 30, 50$ and $80\,\mathrm{GeV}$ corresponds to points from top to bottom. For angle range see text.

The angular dependence of the resolution is shown in Fig. 12. A good uniformity within the total angle range is being observed. The small resolution deterioration have been seen in the real data at high energies (Fig. 5) does not appear in the MC simulation (the bottom set of points in Fig. 12 show flat behaviour). This was expected and means that the simulation program does not describe the details of light collection behind HCAL, i.e. fiber bundles.

Within statistical errors no any coordinate non-uniformity is seen in the simulated data. The effects of light attenuation in the scintillating tiles and fibers due to radiation damage have been studied in [6] and their influence on the HCAL performance has been simulated [8].

8 The tests with 25 ns integrating time electronics

One prototype of a new 40 MHz sampling front-end electronics card [9] has been constructed and tested with HCAL in the 1999 run. A two-fold digitization of the same PMT signal has been implemented for that test. The fast PMT FEU-115M [7] signal was

read out through two 50 Ohm coax cables: a 50 m cable to the LeCroy ADC (gate width ~ 120 ns) and a 10 m cable to the board with the 25 ns integrating cirquit [10].

To satisfy a 25 ns pulse width, a third short cable of 1.1 m terminated with a ~ 23 Ohm resistor was connected to PMT anode to clip the signal tail.

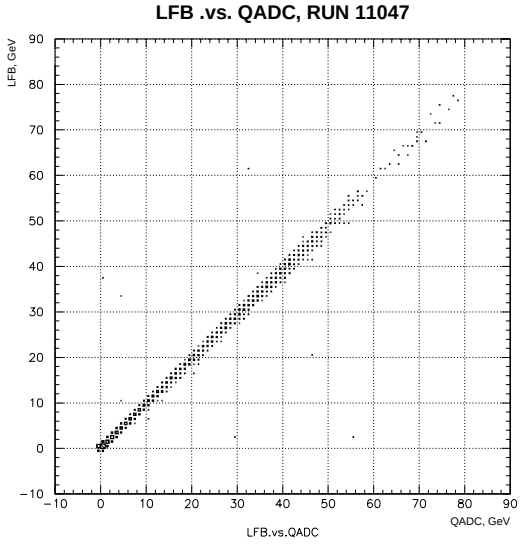

Figure 13: The 25 ns charge integration as compared to LeCroy ADC with a 120 ns gate, measured with HCAL Prototype. In this measurement part of the energy is deposited in the ECAL located in front of HCAL that allow to make a comparison in a wide range of the energy. The beam was 50 GeV.

The plot in Fig. 13 shows a perfect linearity of 40 MHz electronics with respect to the whole charge integrated by an ADC.

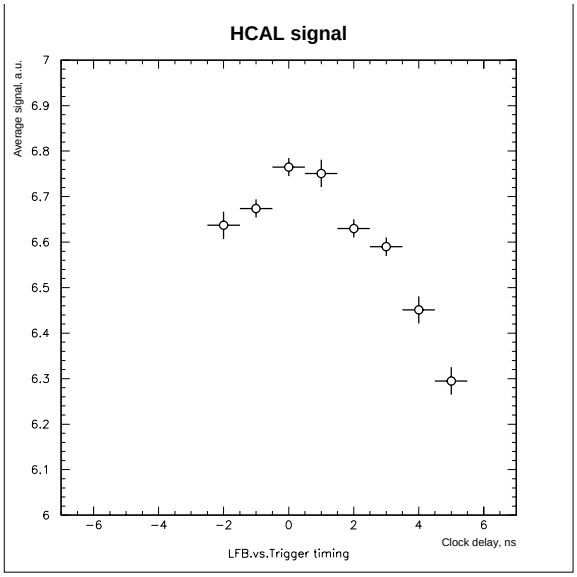

Figure 14: The 40 MHz electronics digitized signal normalized to the ADC signal as a function of the delay between clock and beam particles.

The events have been triggered by the coincidence of beam particles with a 40 MHz clock within ± 5 ns. This time interval has been measured by a TDC and recorded. The fast electronics data being normalized to the ADC data allows to figure out the delay function, shown in Fig. 14. The optimal delay time corresponds to the maximal value of the recorded charge. The shape shown indeed follows the integrating circuit output scanned by a Flash ADC.

9 The combined test with ECAL in front of HCAL

During the 1999 run a first combined test of ECAL and HCAL have been done. To read out both detectors the fast 25 ns sampling electronics was used. The energy dependence of the resolution is shown in Fig. 15.

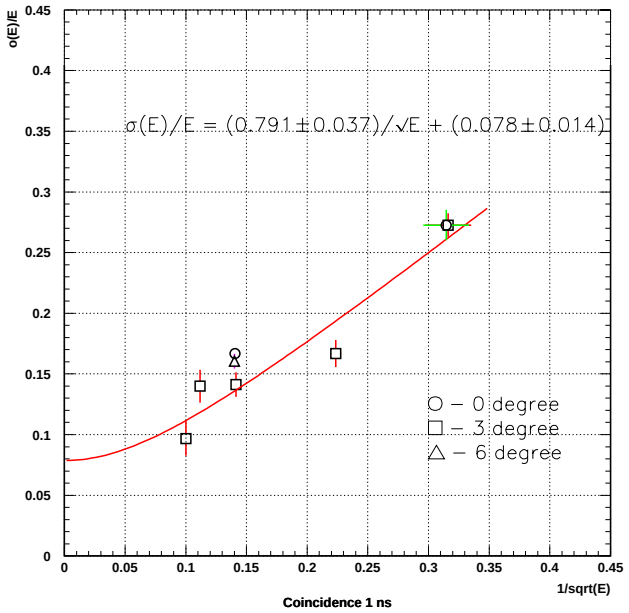

Figure 15: The resolution of the combined ECAL-HCAL calorimeter system.

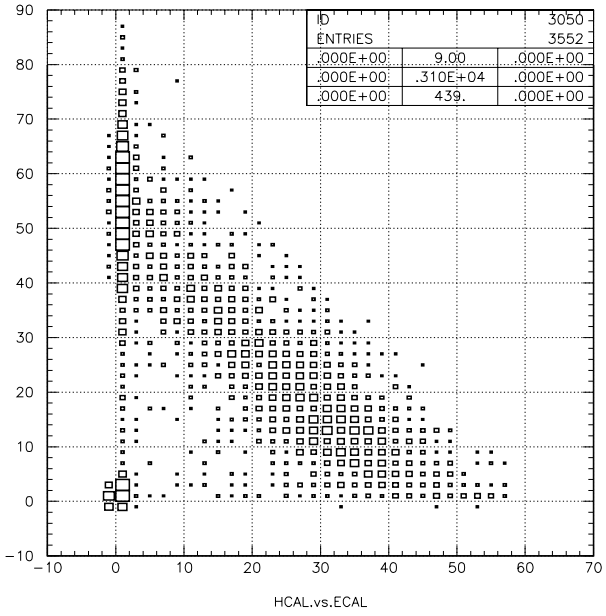

Figure 16: The measured energy plot for the HCAL(Y-axis) versus ECAL(X-axis). The beam energy was 50 GeV. No evidence for a non-linearity is seen when the deposited energy is shared between two detectors.

Even though the statistics collected during that run was limited both by the beam particle - electronics clock coincidence (1/5 of the beam rate) and by the DAQ perfor-

mance it is shown that the measured resolution is in a good agreement with what is required for the LHCb calorimeter system.

The plot shown in Fig. 16 represents the HCAL energy deposition versus one measured in the ECAL. No evidence is seen for a non-linearity when the deposited energy is shared between two calorimeters (so called 'banana-shape') that can appear due to the presence of non-instrumented material between two detectors, e.g. PMT's, supporting structure and so on. Absence of this effect simplifies the energy sum for two calorimeters at the trigger level.

10 The HCAL signal shape study

The main goal of the HCAL is to provide digitized data to the zero level trigger in LHCb. The trigger is based on an event selection with high transverse energy particles. Due to the high L0 decision rate (up to 1 MHz) and large occupancy in the central part of the detector the energy measurement is done within each 25 ns bunch crossing time interval.

This implies strong restrictions on the signal timing. It should be less than 25 ns base to base to allow a complete integration within this time slot.

The HCAL Prototype has been used for shower pulse shape study because it has a large longitudinal dimension that means larger signal jitter.

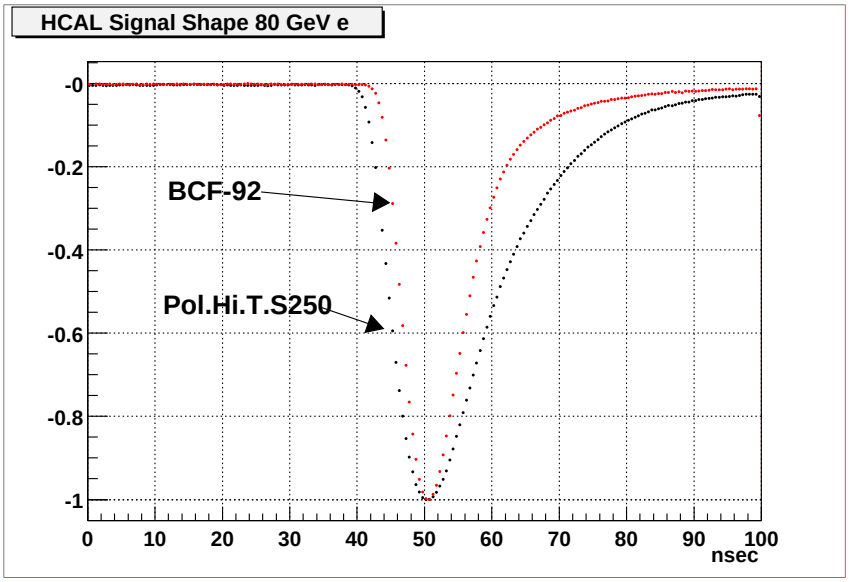

Figure 17: The shape of HCAL Prototype signal recorded by digital scope for cells equipped with two types of fiber.

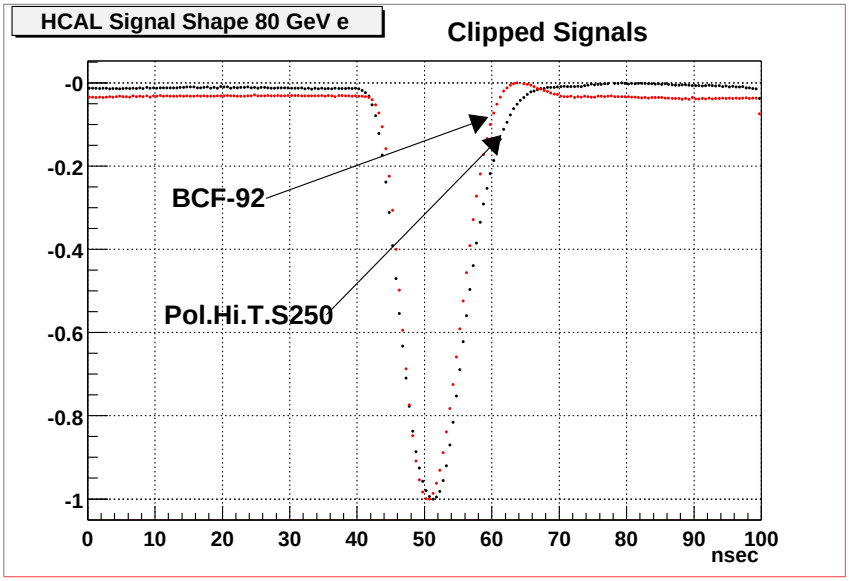

Figure 18: The shape of HCAL Prototype signal after clipping.

The average signal shapes recorded by the fast digital oscilloscope is shown in Fig. 17. All signals measured were taken after 10 m long coaxial cable. Two different HCAL cells instrumented with fibers Pol.Hi.Tech.(S250) and fast BCF-92 were exposed in a 80 GeV electron beam. The light pulses have been detected with PMT FEU-115M.

The evident difference in the fiber decay time is seen, previousely measured with N_2 laser [11]. To satisfy a 25 ns pulse-width requirement the linear clipping cirquit [10] was applied to those signals. The results are shown in Fig. 18.

Both signals are now within 25 ns time slot. Of course, this procedure eventually reduces the signal pulse height especially if a large decay time fibers are in use. This leads to increase of the PMT gain with linearity, aging and stability problems arising. The conclusion is that shorter fiber decay time is better for the HCAL implementation.

This is illustrated by a good result has been obtained with fast BCF-92 fibers in Fig 19. The HCAL signal have been recorded with oscilloscope for 25 ns bunched beam during May'2000 run.

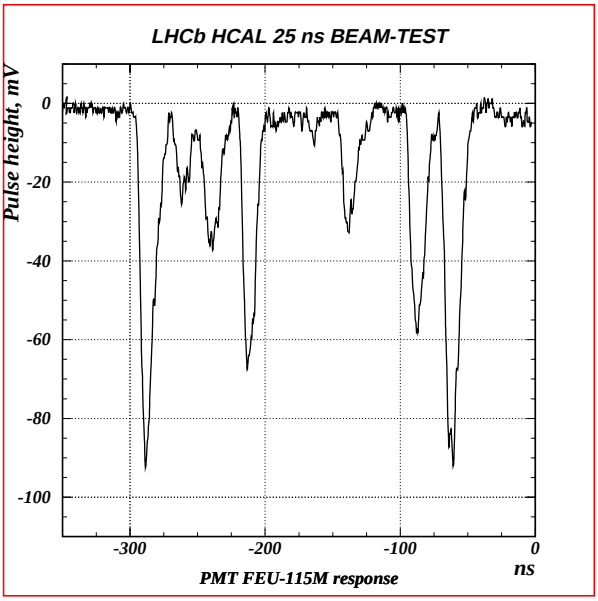

Figure 19: The HCAL signal oscillogram with 25 ns bunched beam.

Clear shower signal separation is seen for several consecutive bunches. Combined with zero dead time integrating front-end electronics [9] this allow to conclude that major requirement to calorimeter system performance has been achieved.

11 Summary

In summary the HCAL Prototype has been tested on the beam to check it's performance as a level zero trigger detector. The linear response is shown with minor correction for the detected energy.

The obtained resolution satisfies the requirements needed for the zero-level trigger purposes. The uniformity in response on X- and Y-coordinates have been shown and no evidence for cracks between modules have been observed.

The light readout from half-tile with single fiber has been tested. The Monte-Carlo simulation describes the general features of the detector.

A calibration procedure with Cs^{137} radioactive source has been developed. The LED pulse system has been developed and tested to monitor the PMT gain stability.

New 40 MHz sampling rate front-end electronics have been used under real experimental environment with the HCAL Prototype. Data have been recorded both with fast electronics and ordinary ADC's for the same event sample and show very well agreement in results.

The signal timing properties have been studied for Prototype instrumented with different fiber types. The conclusion is that the measured HCAL parameters satisfy the performance requirements for LHCb.

Acknowledgements

We are indebted to express our gratitude to CERN SPS accelerator crew and X7 test-beam supporting team for excellent cooperation. We also appreciate worm atmosphere in the LHCb calorimeter group with fruitful discussions and helpful advise. We feel strong support from LHCb and CERN management.

References

[1] LHC-B, Letter of Intent, CERN/LHCC 95-5.

[2] The LHCb Technical Proposal. CERN/LHCC 98-4.

[3] The Hadron Calorimeter Design and Construction.LHCb 2000-45,CALO.

[4] ATLAS Hadron Tile Calorimeter TDR. CERN/LHCC 96-42.

[5] HCAL Prototype Design and Construction, LHCb 2000-35,CALO. LHCb 2000-35,CALO.

[6] HCAL Optics Radiation Damage Study, LHCb 2000-37,CALO.

[7] Study of PMT FEU-115M and FEU-115M-10, LHCb 2000-40,CALO.

[8] HCAL performance with irradiated sub-components, LHCb 2000-38, CALO.

[9] The Front-End Electronics for LHCb Calorimeters, LHCb 2000-28,CALO.

[10] Zero dead-time charge sensitive shaper for calorimeter signal processing, LHCb 2000-041,CALO.

[11] The WLS Fiber Time Properties study, LHCb 2000-39,CALO.